The Journal of Chemical Physics

RESEARCH ARTICLE | FEBRUARY 11 2026

Dipolar cohesion in densely packed confined columns FREE

Yanyu Duan ; Zecheng Gan ; Hervé Mohrbach ; Ho-Kei Chan ; René Messina

J. Chem. Phys. 164, 064905 (2026)
https://doi.org/10.1063/5.0320145

AIP Publishing

The Journal of Chemical Physics ARTICLE pubs.aip.org/aip/jcp

Dipolar cohesion in densely packed confined columns

Cite as: J. Chem. Phys. 164, 064905 (2026); doi: 10.1063/5.0320145
Submitted: 29 December 2025 • Accepted: 28 January 2026 •
Published Online: 11 February 2026

Yanyu Duan,[1] Zecheng Gan,[1,2] Hervé Mohrbach,[3] Ho-Kei Chan,[4,a)] and René Messina[3,b)]

AFFILIATIONS

[1] Thrust of Advanced Materials, and Guangzhou Municipal Key Laboratory of Materials Informatics, The Hong Kong University of Science and Technology (Guangzhou), Guangzhou 511453, China
[2] Department of Mathematics, The Hong Kong University of Science and Technology, Hong Kong SAR, China
[3] Laboratoire de Physique et Chimie Théoriques, LPCT - UMR CNRS 7019, Université de Lorraine, 1 Boulevard Arago, 57070 Metz, France
[4] School of Science, Harbin Institute of Technology (Shenzhen), Shenzhen 518055, China

Note: This paper is part of the JCP Festschrift in Honor of Kurt Kremer.

[a)] **Electronic addresses:** hokeichan@hit.edu.cn and epkeiyeah@yahoo.com.hk
[b)] **Author to whom correspondence should be addressed:** rene.messina@univ-lorraine.fr

ABSTRACT

We investigate theoretically the dipolar cohesion of densely packed columnar assemblies of identical magnetic spheres confined in a cylinder, whose dipole moments are aligned by a tunable strong external magnetic field. Using exact geometrical solutions and dipolar lattice sums, we analyze how the cohesive energy depends on the cylinder diameter. In the zigzag regime, the cohesion exhibits a pronounced nonmonotonic behavior that can be rationalized in terms of competing radial and longitudinal pressures arising from a breaking of ideal head-to-tail dipolar alignment. This competition leads to a point of weakest cohesion, followed by a stabilization of the densest zigzag structure driven by long-range interchain correlations. At larger diameters, a similar bell-shaped evolution of the cohesive energy is found in the helical regime, together with a striking quasi-degeneracy between zigzag and helical morphologies. Our results are directly relevant to experiments on confined dipolar soft matter, ranging from field-responsive magnetic colloids to paramagnetic granular media.

I. INTRODUCTION

Columnar structures arising from the densest packings of identical spheres under cylindrical confinement have been studied for over two decades.[1–15] Such densest-packed structures depend solely on the cylinder-to-sphere diameter ratio D, but not on any absolute length scale. To date, optimal structures have been investigated up to a cylinder-to-sphere diameter ratio of $D = 4.0$,[5] where the vast majority of such structures are chiral. As such, the characterization of densest columnar packings at $D > 4.0$ and their transition toward the bulk limit for increasing D remains an open problem. Such quasi-one-dimensional systems are not only interesting from the theoretical point of view, but they are also of great experimental relevance and importance. They serve as geometric models for the structures of a wide range of systems with fullerenes,[16,17] nanoparticles,[18–20] hollow carbon spheres,[21] colloids,[22–24] microspheres,[25] microbubbles,[26] or polymeric particles[27] in cylindrical confinement and provide a basis for the development of chiral photonic crystals.[28]

On the other hand, the self-assembly of dipolar spheres with the positions and orientations of particles controlled via an externally applied magnetic field has attracted significant attention in recent years, due to potential applications in drug delivery,[29] bioimaging,[30,31] and blood cleansing.[32] In related experiments under quasi-one-dimensional confinement, magnetic colloids can be trapped in a microtube[33] or a microfluidic chip,[34] laying out the possibility of a chain-like cohesion of aligned dipoles that emerges not only in the bulk,[35–39] but also on planar surfaces subjected to an in-plane magnetic field.[40–43] Because such experiments have so far been limited to very narrow cylindrical confinements at $D < 2.0$, the resulting columnar structure of any such system consists of either a single chain[34] or a pair of zippered chains forming a thin two-chain ribbon,[33] with the precise microstructure expected to be dictated by the corresponding cylinder-to-sphere diameter ratio D.

This work elucidates how the cohesive energy of the densest columnar packings of dipolar spheres—confined in a cylindrical geometry and aligned by a strong external magnetic field along the cylinder axis—depends on D. Relying on exact geometrical solutions for the densest-packed structures in the range $D \in [1, 1+3\sqrt{3}/5 \approx 2.039\ 23]$,[14,44,45] we compute accurate cohesive energies per particle and analyze the stability of the competing morphologies. Our results reveal how the cohesive energy is intimately linked to the underlying packing geometry and the resulting dipolar correlations.

The manuscript is organized as follows. Section II introduces the densest columnar structures in the relevant range of D and summarizes the analytical description of their geometry and cohesive energy. In Sec. III, we present the cohesive energy per particle as a function of D and discuss its behavior for the different zigzag and helical morphologies. Section IV concludes the paper and outlines possible extensions. Additional geometrical details and numerical convergence tests are provided in Appendixes A and B.

II. MODEL AND METHODOLOGY

We consider eight types of densest-packed columnar structures formed by equal-sized dipolar hard spheres (with diameter d setting the length scale) confined in a cylindrical pore with diameter ratio $D \in [1,\ 1+3\sqrt{3}/5]$, see Fig. 1. A uniform magnetic field is applied along the cylinder axis (z-direction) and is assumed to be sufficiently strong to align all dipole moments parallel to the field. We first revisit the classification of these densest-packed structures and provide the corresponding analytical solutions for the particle positions, before describing how the cohesive energy of such quasi-one-dimensional assemblies can be evaluated.

A. Densest columnar structures and corresponding analytic solutions

The regime $D \in [1, 1+\sqrt{3}/2)$ is characterized by two interrelated types of densest-packed structures, both sharing a common *coordination number* of 2 (i.e., each sphere touches two nearest neighbors):

(a) **Linear chain**: At $D = 1$, the densest columnar structure is a linear chain of spheres, see Fig. 1(a), in which each sphere is in contact with one sphere above and one sphere below.

(b) **Zigzag**: At $D \in (1, 1+\sqrt{3}/2)$, the densest columnar structure is a planar zigzag with all the sphere centers embedded in the $(x$–$y)$ plane, see Fig. 1(b). As in the case of the linear chain, each sphere remains in contact with two neighboring spheres—one above and one below—albeit laterally shifted. For any pair of adjacent spheres, labeled 1 and 2, the angular separation (twist angle) and the axial displacement are given by

$$\begin{cases} \Delta\phi_{12} = \pi, \\ \Delta z_{12} = \sqrt{1-(D-1)^2}, \end{cases} \tag{1}$$

respectively. As D increases, the vertical separation Δz_{12} decreases monotonically, since the widening of the cylindrical pore allows neighboring spheres to pack more closely along the axial z-direction.

The regime $D \in [1+\sqrt{3}/2, 2)$ encompasses three types of densest-packed structures, all sharing a coordination number of 4:

(c) **Densest zigzag**: At $D = 1+\sqrt{3}/2$, the densest columnar structure is a planar zigzag (hereafter referred to as the densest zigzag), in which each sphere is in contact with four neighboring spheres. As illustrated in Fig. 1(c), this structure can be viewed as two interpenetrating linear chains of spheres. It constitutes the geometric precursor of the twisted configurations that emerge upon further increasing D.

(d) **Single helix**: At $D \in (1+\sqrt{3}/2,\ 1+4\sqrt{3}/7]$, the densest columnar structure is a single helix, in which all adjacent spheres share the same relative geometry, see Fig. 1(d). Each sphere has a coordination number of four, being in contact

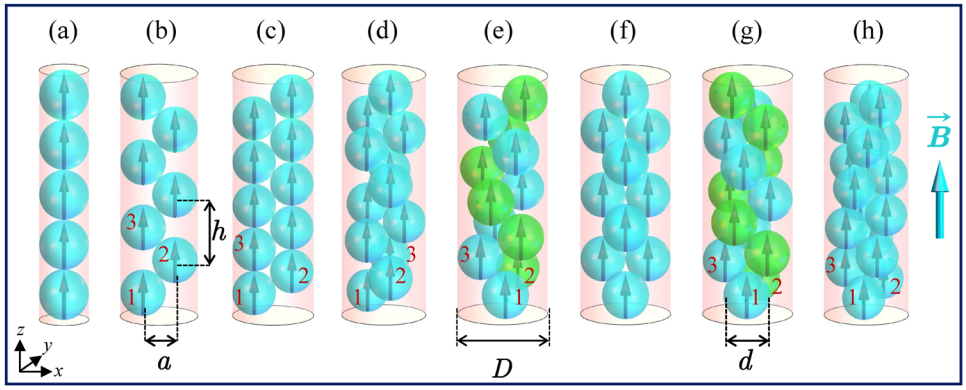

FIG. 1. Densest columnar structures of equal-sized dipolar spheres of diameter $d = 1$, confined inside a cylindrical tube of diameter D and subject to a strong uniform magnetic field $\vec{B} = B\vec{e}_z$: (a) linear chain at $D = 1$; (b) planar zigzag at $D \in (1, 1+\sqrt{3}/2)$; (c) densest planar zigzag at $D = 1+\sqrt{3}/2$; (d) single helix at $D \in (1+\sqrt{3}/2, 1+4\sqrt{3}/7]$; (e) double helix I at $D \in (1+4\sqrt{3}/7, 2)$; (f) achiral doublets at $D = 2$; (g) double helix II at $D \in (2, 1+3\sqrt{3}/5)$; (h) highly coordinated single helix at $D = 1+3\sqrt{3}/5$. Sphere indices increase monotonically along the axial z-direction; (1, 2, 3) are shown for illustration; see also text.

with two neighbors above and two below. The optimal geometry follows from minimizing the axial separation within a triplet of mutually touching spheres, which yields a unique solution for the relative position between adjacent spheres:[14]

$$\begin{cases} \Delta\phi_{12} = \Delta\phi_{23} = \arccos\left(1 - \dfrac{\sqrt{3}}{D-1}\right), \\ \Delta z_{12} = \Delta z_{23} = \sqrt{1 - \dfrac{\sqrt{3}(D-1)}{2}}. \end{cases} \tag{2}$$

(e) **Double helix I**: At $D \in (1 + 4\sqrt{3}/7,\ 2)$, the densest-packed structures are characterized by two distinct geometric solutions for the relative position between adjacent spheres, both resulting from the minimization of the axial separation Δz_{13} of the spanning triplet:[14]

$$\begin{cases} \Delta\phi_{12} = \arccos\left[1 - \dfrac{3(D-1) - f_D}{2(D-1)\left[1 - \sqrt{D(2-D)}\right]}\right], \\ \Delta z_{12} = \sqrt{1 - (D-1)\left\{\dfrac{3(D-1) - f_D}{4\left[1 - \sqrt{D(2-D)}\right]}\right\}}, \end{cases} \tag{3}$$

and

$$\begin{cases} \Delta\phi_{23} = \arccos\left[1 - \dfrac{3(D-1) + f_D}{2(D-1)\left[1 - \sqrt{D(2-D)}\right]}\right], \\ \Delta z_{23} = \sqrt{1 - (D-1)\left\{\dfrac{3(D-1) + f_D}{4\left[1 - \sqrt{D(2-D)}\right]}\right\}}, \end{cases} \tag{4}$$

with

$$f_D \equiv \sqrt{8\left[1 - \sqrt{D(2-D)}\right] - 7(D-1)^2}. \tag{5}$$

This implies that spheres with odd and even indices experience distinct local environments along the helix. As a result, the structure consists of two distinguishable intertwined chains and is therefore classified as a *double helix*; see also Fig. 1(e). We refer to this structure as *double helix I* to distinguish it from the double-helix morphology occurring at $D \in (2, 1 + 3\sqrt{3}/5)$.

For $D \in [2,\ 1 + 3\sqrt{3}/5)$, there exist two types of densest-packed columnar structures with a coordination number of 5:

(f) **Achiral doublets**: At $D = 2$, the densest-packed structure consists of achiral doublets, that is, pairs of spheres sharing the same axial position z, see Fig. 1(f). Successive doublets are rotated by $\pi/2$ in the transverse plane, yielding an overall achiral arrangement. Thereby, each sphere contacts its partner within the same doublet and spheres from the neighboring doublets above and below. The particle positions for this structure can be evaluated using Eqs. (3) and (4), which can be further simplified as

$$\begin{cases} \Delta\phi_{12} = \dfrac{\pi}{2},\ \Delta\phi_{23} = \pi, \\ \Delta z_{12} = \dfrac{1}{\sqrt{2}},\ \Delta z_{23} = 0. \end{cases} \tag{6}$$

(g) **Double helix II**: For $D \in (2, 1 + 3\sqrt{3}/5)$, the densest-packed structure is a double helix composed of tilted doublets, sharing the same coordination number as the achiral doublets,[45] see Fig. 1(g). In this structure, spheres alternate between two distinct local environments: spheres with odd indices $(1, 3, 5, \ldots)$ are in contact with three neighbors above and two below, whereas spheres with even indices $(2, 4, 6, \ldots)$ are in contact with two neighbors above and three below. As in the case of double helix I, the local environment therefore alternates along the column, and the structure is accordingly referred to as double helix II. By accounting for the additional contact with a third-nearest neighbor (e.g., between spheres 1 and 4), together with the double-helix constraint $\Delta\phi_{12} = \Delta\phi_{34}$, we obtain two distinct solutions for the relative position of adjacent spheres:[44]

$$\begin{cases} \Delta\phi_{12} = \arccos\left[1 - \dfrac{4}{3 - \sqrt{9 - 8(D-1)^2}}\right], \\ \Delta z_{12} = \dfrac{\sqrt{1 - \sqrt{9 - 8(D-1)^2}}}{2}, \end{cases} \tag{7}$$

and

$$\begin{cases} \Delta\phi_{23} = 2\pi - \arccos\left[1 - \dfrac{4}{3 + \sqrt{9 - 8(D-1)^2}}\right] \\ \quad - \arccos\left[1 - \dfrac{4}{3 - \sqrt{9 - 8(D-1)^2}}\right], \\ \Delta z_{23} = \dfrac{\sqrt{1 + \sqrt{9 - 8(D-1)^2}} - \sqrt{1 - \sqrt{9 - 8(D-1)^2}}}{2}. \end{cases} \tag{8}$$

(h) **Highly coordinated single helix**: At $D = 1 + 3\sqrt{3}/5$, the densest-packed structure reduces to a single helix in which each sphere has six contacting neighbors—three above and three below along the column axis—so that the coordination number reaches 6, see Fig. 1(h). The relative position between adjacent spheres follows directly from Eqs. (7) and (8) and reads

$$\begin{cases} \Delta\phi_{12} = \Delta\phi_{23} = \arccos\left(-\dfrac{2}{3}\right), \\ \Delta z_{12} = \Delta z_{23} = \dfrac{1}{\sqrt{10}}. \end{cases} \tag{9}$$

B. Dipolar interactions

Under a strong and homogeneous magnetic field $\vec{B} = B\,\vec{e}_z$, these columnar structures can be modeled as dipolar hard spheres with either induced or permanent dipole moments oriented along the z-axis, that is, $\vec{m} = m\,\vec{e}_z$, parallel to the applied field, as illustrated in Fig. 1.

Accordingly, the pair interaction potential U_{ij} between two such dipolar hard spheres, whose centers are located at $\vec{r}_i = (x_i, y_i, z_i)$ and $\vec{r}_j = (x_j, y_j, z_j)$, can be written as

$$U_{ij} = \begin{cases} \frac{\mu_0}{4\pi}\frac{m^2}{r_{ij}^3}\left[1 - 3\frac{(z_j - z_i)^2}{r_{ij}^2}\right], & r_{ij} \geq 1, \\ \infty, & r_{ij} < 1, \end{cases} \tag{10}$$

where $r_{ij} = \|\vec{r}_j - \vec{r}_i\|$.

Choosing a reference particle (say $i = 0$) located at $\left(\frac{D-1}{2}, 0, 0\right)$, the Cartesian coordinates of particle i ($i \in \mathbb{Z}$) can be expressed as

$$\begin{cases} x_i = \frac{D-1}{2}\cos(\phi_i), \\ y_i = \frac{D-1}{2}\sin(\phi_i), \\ z_i = \sum_{k=0}^{i-1}\Delta z_k, \end{cases} \tag{11}$$

where $\phi_i = \sum_{k=0}^{i-1}\Delta\phi_k$ is the cumulated twist angle and z_i is the cumulated axial spacing. The incremental quantities $\Delta\phi_k = \phi_{k+1} - \phi_k$ and $\Delta z_k = z_{k+1} - z_k$ refer to those studied in the previous Sec. II A. For $i < 0$, the sums are understood with reversed bounds.

For a system consisting of N dipolar particles, the total interaction energy reads

$$U_{\text{tot}} = \sum_{i=1}^{N-1}\sum_{j=i+1}^{N} U_{ij}, \tag{12}$$

after a trivial relabeling of indices. In the macroscopic limit ($N \to \infty$), the characteristic reduced energy per particle is then given by

$$u = \frac{1}{N}\frac{U_{\text{tot}}}{U_{\uparrow\uparrow}}, \tag{13}$$

where $U_{\uparrow\uparrow} = \frac{\mu_0 m^2}{4\pi}$ represents the characteristic positive (repulsive) dipolar interaction energy at contact for two spheres in a side-by-side configuration, as suggested by the notation. The convergence of u with respect to N is discussed in Appendix B.

III. RESULTS

Here, we address the intricate behavior of dipolar cohesion at densest packing as a function of the reduced cylinder opening D (see Fig. 2). In the limiting case $D = 1$, the reduced energy per particle reads

$$u_{\text{line}} = -2\zeta(3), \tag{14}$$

for a linear chain, where the Riemann zeta function is defined as $\zeta(s) = \sum_{i=1}^{\infty} i^{-s}$, yielding $\zeta(3) \simeq 1.202$. As the pore size is increased from $D = 1$ to $D = 1 + \sqrt{3}/2$, the linear chain smoothly transforms into a zigzag phase, exhibiting a nontrivial monotonic evolution of the cohesive energy (see Fig. 2). This behavior was previously reported in Refs. 46 and 47, and a corresponding analytical expression was derived by the authors in Ref. 47, namely

$$u_{\text{zigzag}}(D) = -\frac{2}{h^3}\zeta(3) + \frac{2}{h^3}\int_0^{\infty}\exp\left(-\frac{a^2 t}{h^2}\right)\left(\frac{a^2 t}{h^2} - 1\right) \times \theta_3\left(\frac{\pi}{2}, e^{-\pi^2/t}\right)dt, \tag{15}$$

with $h = 2\sqrt{(2-D)D}$ and $a = D - 1$; see also Fig. 1(b) for a geometrical interpretation. Here, θ_3 denotes the Jacobi theta function.[48] Accordingly, (i) the linear chain is recovered for $a = 0$ and $h = 2$, whereas (ii) the densest buckled phase corresponds to $a = \sqrt{3}/2$ and $h = 1$. In addition, an insightful perturbative expansion about the linear chain provides a transparent and exact expression for the energy,

$$u_{\text{zigzag}}(D) = u_{\text{line}} + \left[-3\zeta(3) + \frac{93}{16}\zeta(5)\right]a^2 + \left[-\frac{15}{4}\zeta(3) + \frac{465}{32}\zeta(5) - \frac{5715}{512}\zeta(7)\right]a^4 + \mathcal{O}(a^6), \tag{16}$$

or, numerically,

$$u_{\text{zigzag}}(D) = u_{\text{line}} + 2.420\,971\,867\,a^2 - 0.695\,161\,867\,a^4 + \mathcal{O}(a^6). \tag{17}$$

The pronounced bump observed in the buckled regime can be physically rationalized in terms of two antagonistic effects. On one hand, the linear chain is highly resistant to undulations owing to the strong cohesion associated with the head-to-tail dipolar configuration. This feature is quantitatively captured by Eq. (16); see also Fig. 2. In this context, a negative radial pressure, defined as $-\partial u/\partial D$, reflects a tendency toward radial contraction, which is compensated by a positive longitudinal pressure arising from the frustration of ideal head-to-tail dipolar alignment imposed by geometrical confinement. The dipolar cohesion then becomes weakest at $D = 1 + \sqrt{2}/2 \approx 1.707$, where $a = h/2$ so that $\theta_{12} = \pi/4$, yielding a maximum reduced energy $u \simeq -1.577$ as a direct extremization of Eq. (15) or its equivalent lattice sum given by Eq. (12). At this point, the effective radial pressure $-\partial u/\partial D$ vanishes, identifying an unstable mechanical equilibrium of the confined column.

On the other hand, as the system approaches the densest zigzag configuration—that is, for $1 + \sqrt{2}/2 < D < 1 + \sqrt{3}/2$—an additional gain in cohesion arises from interchain attractive correlations, which are long-range in nature.[42,49] In this regime, the effective radial pressure becomes positive, reflecting a tendency of the dipolar column to expand radially as cohesion is restored. The densest zigzag structure constitutes a key ground state of the present problem, and its associated energy is given by

$$u_{\triangle} = u_{\text{zigzag}}(D = 1 + \sqrt{3}/2) \simeq -2.581\,884. \tag{18}$$

More specifically, when $1.8572 < D < 1 + \sqrt{3}/2 \simeq 1.8660$, the zigzag structure becomes the *overall ground state* and overtakes the linear chain, as established in Ref. 47; see also Fig. 2.

In the helical regime where $1 + \sqrt{3}/2 < D < 1 + 3\sqrt{3}/5$, the dipolar cohesion again exhibits a nonmonotonic dependence on D, reminiscent of the bell-shaped behavior observed in the zigzag regime, and can be interpreted in terms of a similar behavior of

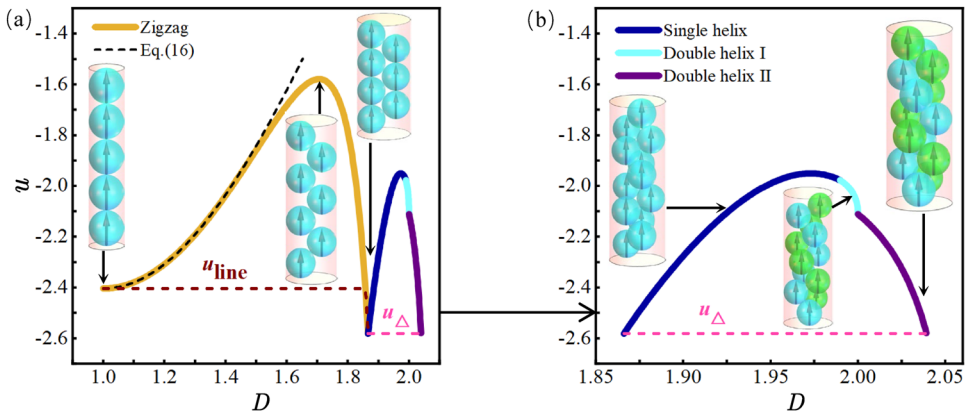

FIG. 2. Cohesive energy per particle u as a function of D. (a) Overview including the zigzag and helical structures. The energies of the linear chain u_{line} and of the dense zigzag $u_\triangle$ are shown for reference. The zigzag energy is computed from its analytical integral representation given by Eq. (15). The perturbative expansion about the linear chain is also shown for comparison, as given by Eq. (16). (b) The helical regime is shown separately for the sake of clarity.

the effective radial pressure. For the single-helix structure vivid at $1 + \sqrt{3}/2 < D < 1 + 4\sqrt{3}/7$; upon departing from the zigzag configuration, the vertical spacing between successive particles along the helix decreases smoothly from $\overline{\Delta z} = 0.5$, see Fig. 4 (Appendix A), to optimize packing.[12] Simultaneously, the twist angle $\Delta\phi$ decreases continuously from π, see Fig. 5 (Appendix A). This optimal packing arrangement as a function of D leads to a gradual loss of cohesion, reflected by an increase in the reduced energy u (see Fig. 2) as a direct consequence of the dipolar energetic cost associated with the further undulation of the structure. The energy of the single-helix structure culminates at $D \simeq 1.973$, when the mean internal height approaches its minimal value, $\overline{\Delta z} \simeq 0.378$, at which $u \simeq -1.950$; see Fig. 4 (Appendix A) and Fig. 2, respectively.

To account for the recovery of cohesion associated with double helices at larger D, we introduce the *local helical dipolar energy*,

$$\tilde{U}_{\rm loc} \equiv \frac{U_{12} + U_{23}}{2} = 1 - 3\overline{(\Delta z)^2}, \tag{19}$$

where U_{12} and U_{23} denote the dipolar interaction energies between successive nearest neighbors along the helical column. The new geometrical order parameter $\overline{(\Delta z)^2}$, entering Eq. (19), quantifies the mean squared axial separation between successive neighbors and is defined as

$$\overline{(\Delta z)^2} = \frac{(\Delta z_{12})^2 + (\Delta z_{23})^2}{2}. \tag{20}$$

Its dependence on D is shown in Fig. 3. Hence, the characteristic loss and subsequent recovery of dipolar cohesion across the single-helix-to-double-helix transition are fully consistent with the corresponding evolution of $\overline{(\Delta z)^2}$ (compare Fig. 2 with Fig. 3). This local interaction picture thus provides a satisfactory explanation for the bell-shaped dependence of u. However, the further decrease of u (i.e., the increase in cohesion) observed for double helices II, which becomes prominent for $2 < D < 1 + 3\sqrt{3}/5$, cannot be captured within a purely local energy argument; compare Fig. 2 with Fig. 3. In this regime, the highly intricate long-range and anisotropic nature of dipolar interactions must be taken into account to rationalize the additional stability. Although the dense zigzag configuration corresponds to the lowest-energy state, its energy is found to be extremely close (within less than a 10^{-3} relative difference) to that of the helical structure at larger $D = 1 + 3\sqrt{3}/5$, indicating an intriguing quasi-degeneracy between these competing morphologies.

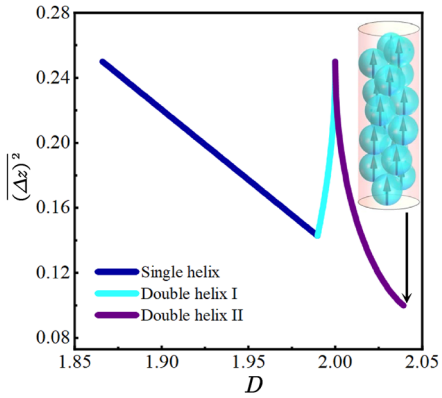

FIG. 3. Mean squared axial separation $\overline{(\Delta z)^2}$ as a function of D.

IV. CONCLUDING REMARKS

In conclusion, we have shown that the dipolar cohesion of densely packed confined columns is governed by a subtle interplay between geometrical constraints and long-range dipolar correlations. Our analytical expressions for the zigzag cohesion and the identification of effective radial and longitudinal pressures provide direct physical insights beyond what can be inferred from purely numerical or packing-based approaches alone. In the zigzag regime, $1 < D < 1 + \sqrt{3}/2$, the nonmonotonic dependence of the cohesion energy on the confinement diameter D can be rationalized in terms of competing radial and longitudinal pressures originating from the breaking of the ideal head-to-tail dipolar alignment imposed by cylindrical confinement. This competition leads to a point of weakest cohesion where the radial pressure vanishes. Upon further confinement, long-range interchain correlations restore cohesion and stabilize the densest zigzag structure, in agreement with earlier findings.[39,46,47,49]

In the helical regime, $1 + \sqrt{3}/2 < D < 1 + 3\sqrt{3}/5$, a similar bell-shaped evolution of the cohesive energy is observed. We show that its initial behavior can be captured by a local geometrical order parameter, while the enhanced stability of double helices at larger D reflects the intrinsically long-range nature of dipolar interactions.[42] Notably, we uncover a striking quasi-degeneracy between the densest zigzag and helical morphologies, highlighting the delicate energetic balance that governs confined dipolar matter.

These findings are expected to be directly relevant for experiments on magnetically aligned colloids confined in microtubes[33] or capillaries,[50] where dipolar chains, zigzag ribbons, and helical structures are routinely observed under external magnetic fields. The predicted nonmonotonic evolution of cohesion with confinement, as well as the near-degeneracy between competing morphologies, may manifest experimentally through structural coexistence, enhanced fluctuations, or sensitivity to external magnetic fields.

More broadly, our approach can be extended to larger confinement diameters, tilted or rotating external fields, and electrically dipolar or magnetoelectric systems, opening the way to a systematic understanding of cohesion and stability in quasi-one-dimensional dipolar matter.

ACKNOWLEDGMENTS

R.M. expresses his sincere gratitude to Kurt Kremer for the precious years spent in Mainz and for opening the door to the fascinating world of soft matter physics. Z.G. and Y.D. acknowledge the support from the Natural Science Foundation of China (Grant No. 12201146) and the Guangzhou-HKUST(GZ) joint research project (Grant Nos. 2023A03J0003 and 2024A03J0606). H.K.C. would like to acknowledge financial support from the Guangdong Basic and Applied Basic Research Foundation, China (Grant No. 2024A1515011585).

AUTHOR DECLARATIONS

Conflict of Interest

The authors have no conflicts to disclose.

Author Contributions

Yanyu Duan: Data curation (equal); Writing – original draft (equal); Writing – review & editing (equal). **Zecheng Gan**: Supervision (lead); Writing – review & editing (supporting). **Hervé Mohrbach**: Formal analysis (supporting); Writing – review & editing (supporting). **Ho-Kei Chan**: Conceptualization (equal); Formal analysis (equal); Methodology (equal); Supervision (equal); Writing – original draft (supporting); Writing – review & editing (supporting). **René Messina**: Conceptualization (equal); Formal analysis (equal); Writing – original draft (lead); Writing – review & editing (equal).

DATA AVAILABILITY

The data that support the findings of this study are available from the corresponding author upon reasonable request.

APPENDIX A: RELEVANT ORDER PARAMETERS FOR HELICAL STRUCTURES

1. Effective axial spacing

We introduce the *effective axial spacing*,

$$\overline{\Delta z} = \frac{\Delta z_{12} + \Delta z_{23}}{2}, \tag{A1}$$

which provides a convenient measure of the axial compaction of the structure. Note that for single helices, the effective axial spacing reduces to $\overline{\Delta z} = \Delta z_{12} = \Delta z$. The resulting profile of $\overline{\Delta z}(D)$ is obtained by inserting the related expressions of Δz_{12} and Δz_{23} derived in Sec. II A (see Fig. 4). There, $\overline{\Delta z}$ decreases monotonically with increasing D, reflecting an enhanced axial compaction enabled by radial displacements. At the local level, the concomitant increase of the reduced energy originates from the increasing deviation of dipolar pair orientations from the field axis.

2. Effective twist angle

We jointly introduce the *effective twist angle*,

$$\overline{\Delta\phi} = \frac{\Delta\phi_{12} + \Delta\phi_{23}}{2}, \tag{A2}$$

which provides a convenient geometric measure of the average azimuthal winding of the column around the cylinder axis. Notice that for single helices, the effective twist angle reduces to $\overline{\Delta\phi} = \Delta\phi_{12} = \Delta\phi$. The resulting profile of $\overline{\Delta\phi}(D)$ is obtained by inserting the related expressions of $\Delta\phi_{12}$ and $\Delta\phi_{23}$ derived in Sec. II A (see Fig. 5). There, $\overline{\Delta\phi}$ decreases monotonically with increasing D, reflecting the progressive relaxation of radial confinement, which reduces the azimuthal winding required to maintain the densest packing.

APPENDIX B: CONVERGENCE ANALYSIS

The relative error $|\Delta u/u|$ as a function of the system size N for representative densest columnar structures is depicted in Fig. 6. Here,

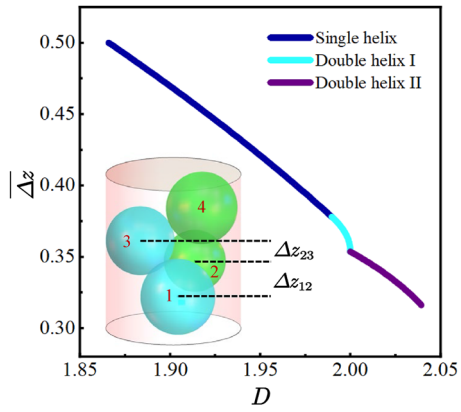

FIG. 4. Order parameter $\overline{\Delta z}$ vs D. The inset illustrates the internal axial separations Δz_{12} and Δz_{23}.

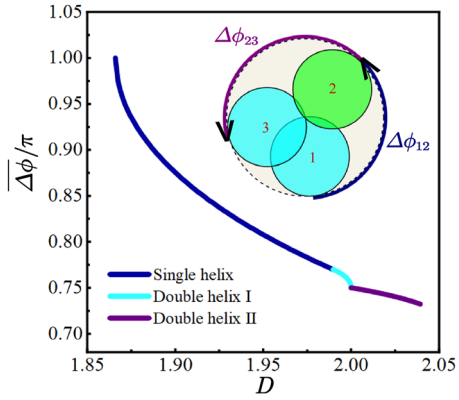

FIG. 5. Order parameter $\overline{\Delta\phi}$ vs D. The inset provides a top view illustrating the internal twist angles $\Delta\phi_{12}$ and $\Delta\phi_{23}$.

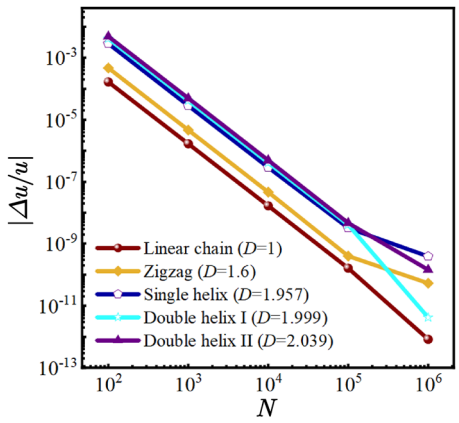

FIG. 6. Relative error $|\Delta u/u|$ as a function of the system size N for representative columnar structures.

$$\Delta u \equiv u_N - u_\infty, \tag{B1}$$

where u_∞ is estimated from the converged value at $N_{\text{conv}} = 10^7$ (see also Fig. 6). At a prescribed system size N, $|\Delta u/u|$ generally increases with D, reflecting larger finite-size corrections in the more complex (helical and multi-strand) morphologies. In light of this observation, all energies u reported in this work are computed using at least 10^5 particles.

REFERENCES

[1] J. Winkelmann and H.-K. Chan, *Columnar Structures of Spheres: Fundamentals and Applications* (Jenny Stanford Publishing, Singapore, 2023).
[2] H.-K. Chan, Phys. Rev. E **84**, 050302(R) (2011).
[3] H.-K. Chan, Philos. Mag. **93**, 4057 (2013).
[4] F. J. Durán-Olivencia and M. C. Gordillo, Phys. Rev. E **79**, 061111 (2009).
[5] L. Fu *et al.*, Soft Matter **12**, 2505 (2016).
[6] L. Fu *et al.*, Soft Matter **13**, 3296 (2017).
[7] K. Koga and H. Tanaka, J. Chem. Phys. **124**, 131103 (2006).
[8] M. A. Lohr *et al.*, Phys. Rev. E **81**, 040401 (2010).
[9] A. Mughal, H. K. Chan, and D. Weaire, Phys. Rev. Lett. **106**, 115704 (2011).
[10] A. Mughal, H. K. Chan, D. Weaire, and S. Hutzler, Phys. Rev. E **85**, 051305 (2012).
[11] A. Mughal, Philos. Mag. **93**, 4070 (2013).
[12] G. T. Pickett, M. Gross, and H. Okuyama, Phys. Rev. Lett. **85**, 3652 (2000).
[13] M. Z. Yamchi and R. K. Bowles, Phys. Rev. Lett. **115**, 025702 (2015).
[14] H.-K. Chan, Y. Wang, and H. Han, AIP Adv. **9**, 125118 (2019).
[15] A. Mughal and D. Weaire, Phys. Rev. E **89**, 042307 (2014).
[16] A. N. Khlobystov, D. A. Britz, A. Ardavan, and G. A. D. Briggs, Phys. Rev. Lett. **92**, 245507 (2004).
[17] W. Mickelson *et al.*, Science **300**, 467 (2003).
[18] S. Sanwaria *et al.*, Angew. Chem., Int. Ed. **53**, 9090 (2014).
[19] V. T. Cong *et al.*, J. Am. Chem. Soc. **136**, 3833 (2014).
[20] R. Liang *et al.*, ACS Macro Lett. **3**, 486 (2014).
[21] Z. Chen *et al.*, Small **14**, 1704015 (2018).
[22] F. Li, X. Badel, J. Linnros, and J. B. Wiley, J. Am. Chem. Soc. **127**, 3268 (2005).
[23] J. H. Moon *et al.*, Langmuir **20**, 2033 (2004).
[24] M. Tymczenko *et al.*, Adv. Mater. **20**, 2315 (2008).
[25] S. A. Vanapalli *et al.*, Langmuir **24**, 3661 (2008).
[26] A. Meagher *et al.*, Colloids Surf. A **473**, 55 (2015).
[27] T. Lee, K. Gizynski, and B. A. Grzybowski, Adv. Mater. **29**, 1704274 (2017).
[28] T. Liu, H.-K. Chan, and D. Wan, Soft Matter **19**, 7313 (2023).
[29] J. D. G. Durán, J. L. Arias, V. Gallardo, and A. V. Delgado, J. Pharm. Sci. **97**, 2948 (2008).
[30] N. A. Frey, S. Peng, K. Cheng, and S. Sun, Chem. Soc. Rev. **38**, 2532 (2009).
[31] G. K. Das *et al.*, Chem. Mater. **23**, 2439 (2011).
[32] C. W. Yung, J. Fiering, A. J. Mueller, and D. E. Ingber, Lab Chip **9**, 1171 (2009).
[33] P. Liu, J. W. J. de Folter, A. V. Petukhov, and A. P. Philipse, Soft Matter **11**, 6201 (2015).
[34] F. Lacharme, C. Vandevyver, and M. A. M. Gijs, Microfluid. Nanofluid. **7**, 479 (2009).
[35] R. Tao and J. M. Sun, Phys. Rev. Lett. **67**, 398 (1991).
[36] T. C. Halsey, Science **258**, 761 (1992).
[37] U. Dassanayake, S. Fraden, and A. van Blaaderen, J. Chem. Phys. **112**, 3851 (2000).
[38] A.-P. Hynninen and M. Dijkstra, Phys. Rev. Lett. **94**, 138303 (2005).
[39] L. Spiteri and R. Messina, Phys. Rev. Lett. **119**, 155501 (2017).
[40] J. J. Weis, Mol. Phys. **103**, 7 (2005).
[41] A. Darras *et al.*, Eur. Phys. J. E **39**, 47 (2016).
[42] R. Messina and I. Stanković, Physica A **466**, 10 (2017).
[43] E. Kemgang and R. Messina, Phys. Rev. E **105**, L012602 (2022).
[44] Y. Wang, M.S. thesis, Harbin Institute of Technology, Shenzhen, China, 2018.
[45] P. Ma and H.-K. Chan, Front. Phys. **9**, 778001 (2021).
[46] F. Deißenbeck, H. Löwen, and E. C. Oğuz, Phys. Rev. E **97**, 052608 (2018).
[47] A. Mourad, H. Mohrbach, and R. Messina, Europhys. Lett. **141**, 67001 (2023).
[48] M. Abramowitz and I. A. Stegun, *Handbook of Mathematical Functions with Formulas, Graphs, and Mathematical Tables* (Dover Publications, New York, 1972).
[49] R. Messina and L. Spiteri, Eur. Phys. J. E **39**, 81 (2016).
[50] E. Cereceda-López *et al.*, Soft Matter **20**, 7615 (2024).